J. Plasma Physics (2011), *vol.* 77, *part* 4, *pp.* 479–491.
doi:10.1017/S0022377810000656

Turbulence changes in laser enhanced laser induced plasmas

D. L. WIGGINS, C. T. RAYNOR and J. A. JOHNSON, III

Center for Plasma Science and Technology, Florida A & M University,
Tallahassee, FL 32310, USA
(wiggins@cepast.famu.edu)

(Received 21 September 2010; revised 14 October 2010; accepted 16 October 2010;
first published online 15 November 2010)

Abstract. A neodymium-doped yttrium aluminum garnet laser of wavelength 0.532 μm with the maximum energy of 900 mJ creates plasmas at a focal point in air in the path of a 1 kW continuous wave fiber laser of wavelength 1.08 μm. We find that there is an unexpected influence on a standard set of turbulent parameters in these laser-induced plasmas. Specifically, the continuous wave laser increased the complexity in the turbulent fluctuations. The continuous wave laser reduces the characteristic fluctuation frequencies in the neutral lines. Furthermore, the continuous wave laser enhances turbulence energies in ions while it diminishes turbulence energies in neutrals.

1. Introduction

Turbulent effects have been observed in plasmas produced by arc-driven shock waves, microwave generated plasmas, moving and stationary plasmas, and in laser-induced plasmas [1–4]. However, no research has gone into understanding the turbulent environment of a laser-induced plasma produced directly in the path of a high irradiance continuous wave (cw) laser. Since turbulence is a well-known collective effect, it seems appropriate to explore the possibilities of new physics that might come from studying a laser enhanced laser-induced plasma where the collective motions associated with laser oscillations might couple with turbulent phenomena. In general, new effects could have broad implications for the development of new turbulence physics, for the manipulation of turbulence transport, for the fundamental physics of high-energy systems, and for new technologies inherently increasing the visibility (signal-to-noise ratio) of spectra of interest by provoking indentifying unique behaviors.

Turbulence has been defined as a state of random and chaotic motions, which appear unpredictable [5]. No complete quantitative theory of turbulence has yet been evolved [6]. However, we have recently developed a set of techniques in our laboratory where transition to turbulence is understood by the use of the Ginzburg–Landau second order phase transformation [7]. This approach focuses attention on phase space trajectories, characterizing frequencies in fluctuation power spectrum and on the role of critical turbulent energy concepts in the observed change in transport parameters. The Ginzburg–Landau approach along with Kolmogorov's approach based on cascading eddies [5] rationalizes for us a standard set of turbulent parameters. Specifically, we use the chaotic dimension, the turbulent energy, the

spectral index and the characteristic fluctuation frequency. The techniques used to derive these parameters from the fluctuations of the plasma signal will be discussed below.

2. Analytical techniques

From successes in the treatment of superconductivity, when the Ginzburg–Landau theory [8] is used to explain the transition from non-turbulent to turbulent behavior in our plasma specific behaviors are predicted. In particular, when a transport parameter is plotted versus the turbulent energy, a lambda-like behavior is shown. From these plots we can distinguish a critical turbulent energy that is associated with the phase transition.

The complexity of a turbulent system is determined by its second Hausdorff dimension [9], which we define as its chaotic dimension. The chaotic dimension is the lowest number of variables needed to completely characterize a system. By taking the phase space trajectory of the fluctuations created by plasma signal we can then estimate the chaotic dimension. Using the following correlation integral

$$C(r) = \lim_{N\to\infty} \frac{1}{N^2} \sum^{N} \theta\left(r - \left|\vec{X}_i - \vec{X}_j\right|\right), \tag{1}$$

where θ is the Heaviside step function keeping count of the number of time the value of scaling length r is larger than the distance between two points in phase space X_i and X_j. When the value of the scaling length r is small the correlation integral becomes

$$C(r) = r^{D_2}, \tag{2}$$

where D_2 is the chaotic dimension [10].

The turbulent energies and characteristic frequencies are determined directly from the Fourier power spectra of the turbulent fluctuations. Specifically, to obtain the power spectrum $P(\omega)$ of the plasma we take the Fourier transform of the fluctuations of the plasma signal as captured. The power spectrum is a plot of the power verses the frequency. Turbulent energy is defined as the integration of the power spectrum $P(\omega)$ over ω_i up to the noise regime

$$E_\tau = \sum_{\omega=\omega_i}^{\omega_i=noise} P(\omega), \tag{3}$$

where ω_i is the frequency. The turbulent energy provides a systematic way to determine the total strength of the fluctuations in the signal [4]. The characteristic frequency is the value of the strongest frequency in the power spectrum.

Taking the log–log plot of the Fourier power spectrum from fluctuations of the system, we then divide the plot up into four regions: the energy input region, the Kolmogorov region, the high frequency region, and the noise region. In the inertial range of energy spectrum the Kolmogorov power law is

$$E(k,t) = C\varepsilon^{-2/3}k^{-5/3}. \tag{4}$$

The Kolmogorov $-5/3$ law is a well-known prediction of how, under ideal circumstances, the energy spectrum evolves in the inertial range [11]. Applying this

https://doi.org/10.1017/S0022377810000656 Published online by Cambridge University Press

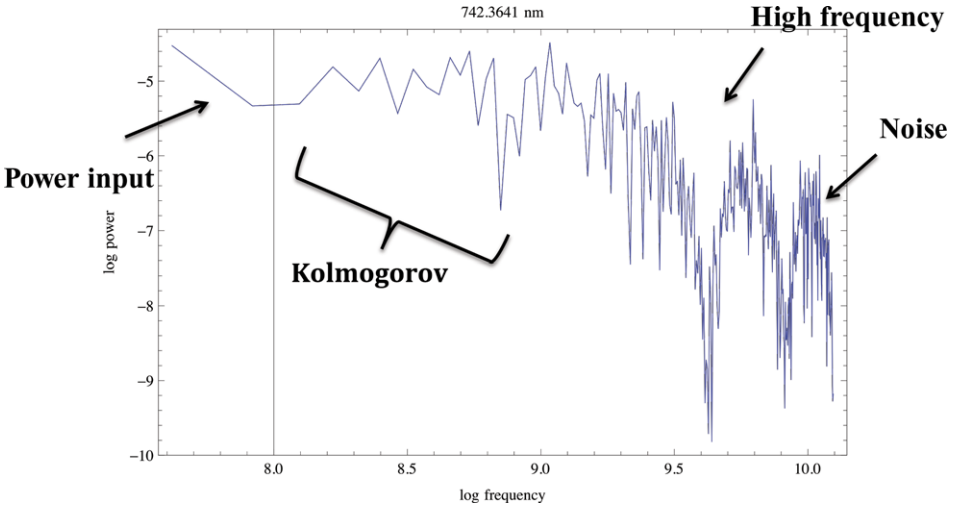

Figure 1. (Colour online) The log–log plot of the Fourier power spectrum from fluctuations of the system and then we divide the plot up into four regions: the energy input region, the Kolmogorov region, the high frequency region, and the noise region. Here we see, using $P = \omega^{-n}$ in that region, a value for $n = 1.91 \pm 0.232$ as the spectral index from Kolmogorov's power law.

law to our power spectrum results yield that the spectral index is the index n in

$$P = \omega^{-n}, \tag{5}$$

where n is the slope of the Kolmogorov region. Here the spectral index is the rate at which the energy propagates through the length scales [12, 13]. Thus n qualifies as a transport parameter

$$n = \frac{(-dP/P)}{(d\omega/\omega)}, \tag{6}$$

where P is the power and ω is the frequency. For example, in Fig. 1, the spectral index, the rate at which the energy propagates through the length scales [14, 15], is found to be $n = 1.91 \pm 0.232$. In the Kolmogorov region, one has for most systems $-1 \leqslant n \leqslant -7$ [16].

3. Experimental setup

The overall experimental setup is sketched in Fig. 2. The experimental setup includes a neodymium: yttrium-aluminum-garnet (Nd:YAG) pulse laser with a wavelength of 0.532 μm and maximum energy of 500 mJ. The lens used in our LELIP experiment has a focal length of 15 cm. The duration of the Nd:YAG laser pulse is 6–8 ns. The minimum power is 240.1 mJ, the maximum power is 249.9 mJ, and the mean is 244.7 mJ. Thus, the measured standard deviation in the laser pulse power is 3.371 mJ. The calculated irradiance of the Nd:YAG laser is 2.08×10^{11} W cm^{-2}. To keep track of the pulse laser power we placed a beam splitter in the bath of the laser beam. The beam splitter is turned to a 45-degree angle in order to send half of the beam to a power meter. The power meter allows us to keep track of the power of each pulse generated by the Nd:YAG laser.

https://doi.org/10.1017/S0022377810000656 Published online by Cambridge University Press

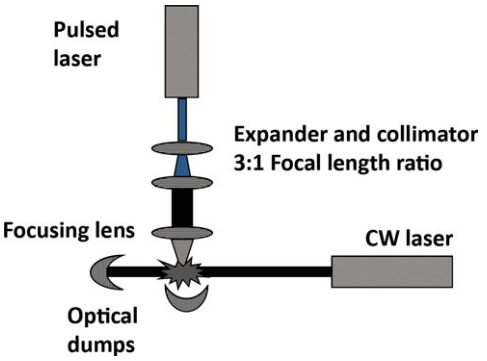

Figure 2. (Colour online) A schematic drawing of the laser enhanced laser induced plasma experiment.

The cw fiber laser properties are a wavelength of 1.08 μm, a maximum power of 1 kW and a beam diameter of 2 cm. The purpose of the cw fiber laser is to bath the plasma created by the Nd:YAG laser and to manipulate the turbulent effects of the laser-induced plasmas. The plasma is located at a fixed position and the irradiance of the cw fiber laser is increased in equal steps. The irradiance is the power per unit area at the plasma. The position of the cw beam is perpendicular to the plasma and is also in a fixed position. The plasma is created exactly in the middle of the cw beam.

These emissions are then sent to a photomultiplier tube (PMT) used to capture the emission of the neutral and ionic nitrogen lines from the Y-shaped fiber optic cable. The Tektronix digitizing oscilloscope that is used to capture the signal of the plasma sent through the PMT has a sampling speed of $50\,\mathrm{GS\,s^{-1}}$. The turbulent analysis is performed on data collected on the oscilloscope of the laser-induced plasma being bathed by the cw fiber laser. The date rate of the oscilloscope is extremely important since the plasmas we create are on the order of nanoseconds duration. We choose air as the target medium; first of all, because the general features of laser induced turbulent plasmas in air are well understood [4].

4. Results and discussion

A Mathematica 7 code is used to calculate all of the turbulent parameters (i.e. turbulent energy, spectral index, characteristic frequency, and chaotic dimension). From our results, we have found that, as the irradiance increases, there are significant changes in these turbulent parameters. In Fig. 3 the complexity of the plasma increases for the neutral line as the cw laser increases. Visually we observe that the phase space trajectory winds more tightly around the axes as the irradiance increase. Thus, the number of variables needed to describe the plasma increases for the neutral nitrogen line.

Figure 4 shows the shift in the strongest peak position as the cw laser changes from $96\,\mathrm{W\,cm^{-2}}$ to $286\,\mathrm{W\,cm^{-2}}$. Recall, that the characteristic frequency is the position of the strongest peak of the power spectrum. Figure 5 shows that the characteristic frequency for the neutral line generally decreases as the cw laser irradiance increases.

Figure 6 shows that the area under the power spectrum decreases for the neutral line as the cw laser irradiance changes from $96\,\mathrm{W\,cm^{-2}}$ to $286\,\mathrm{W\,cm^{-2}}$. Figure 7

https://doi.org/10.1017/S0022377810000656 Published online by Cambridge University Press

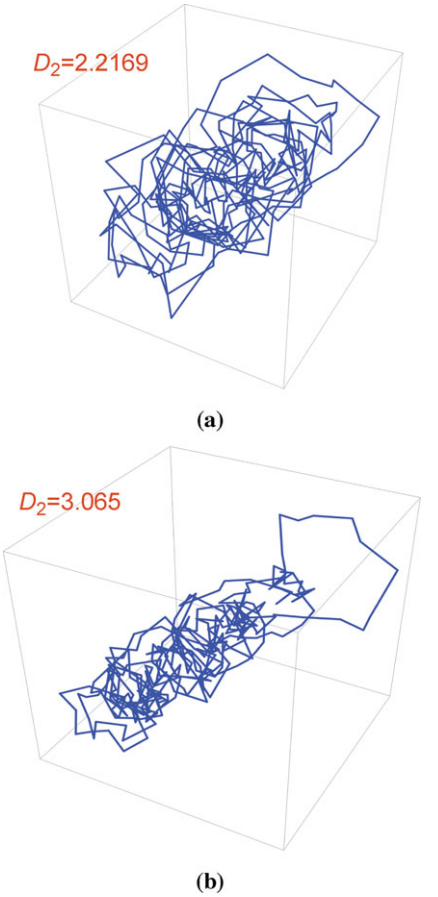

Figure 3. (Colour online) These plots show the effect that the continuous wave (cw) laser has on the complexity of the plasma of the neutral line as the irradiance changes (a) 96 W cm^{-2} to (b) 286 W cm^{-2} for $t = 350$ ns.

shows that the area under the power spectrum increases for the ion line as the cw laser irradiance changes from 96 W cm^{-2} to 286 W cm^{-2}. Recall, the turbulent energy is the integral of the power spectrum up to noise. As seen in Fig. 8 the turbulent energy decreases for the neutral line and increases for the ion line as the cw fiber laser irradiance increases. The enhancement to the ion energy is probably due to inverse bremsstrahlung [17] which provides energizing collisions between the electrons and the positive ions. The decrease in the neutral energies is probably also a byproduct of inverse bremsstrahlung since the energetic neutrals can be more easily excited to higher states (alternative to the neutral line being monitored) by the electrons and thereby reduce the overall energy content of the neutral species being tracked. This suggests that the cw laser strengthens the fluctuations of the ion line and diminishes the fluctuation strength of the neutral line.

In all cases, laser enhanced laser-induced plasmas show consistent evidence of a useful second-order transformation interpretation for turbulence. When plotting spectral index verses turbulent energy for the ion line we observed a lambda-like

https://doi.org/10.1017/S0022377810000656 Published online by Cambridge University Press

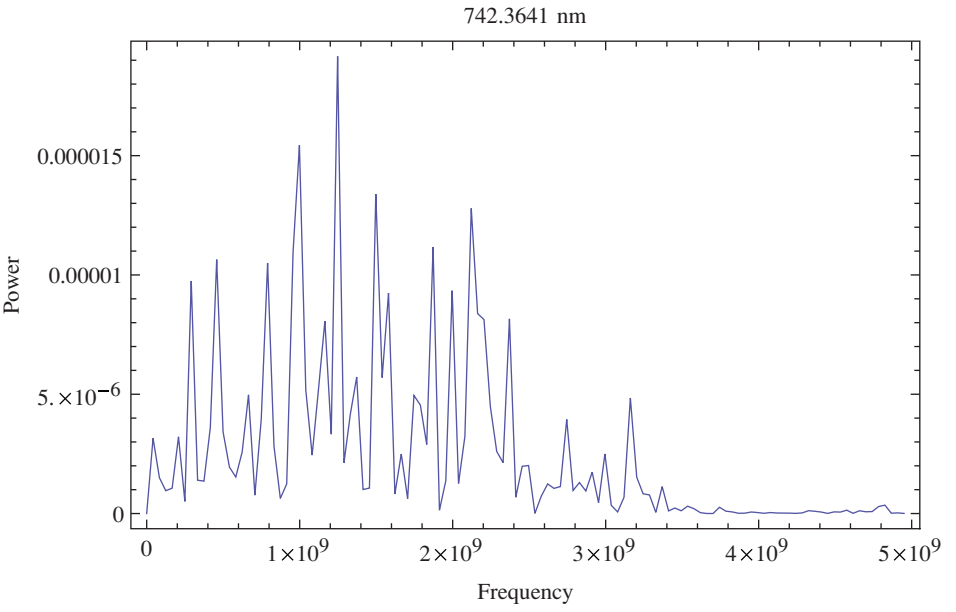

(a)

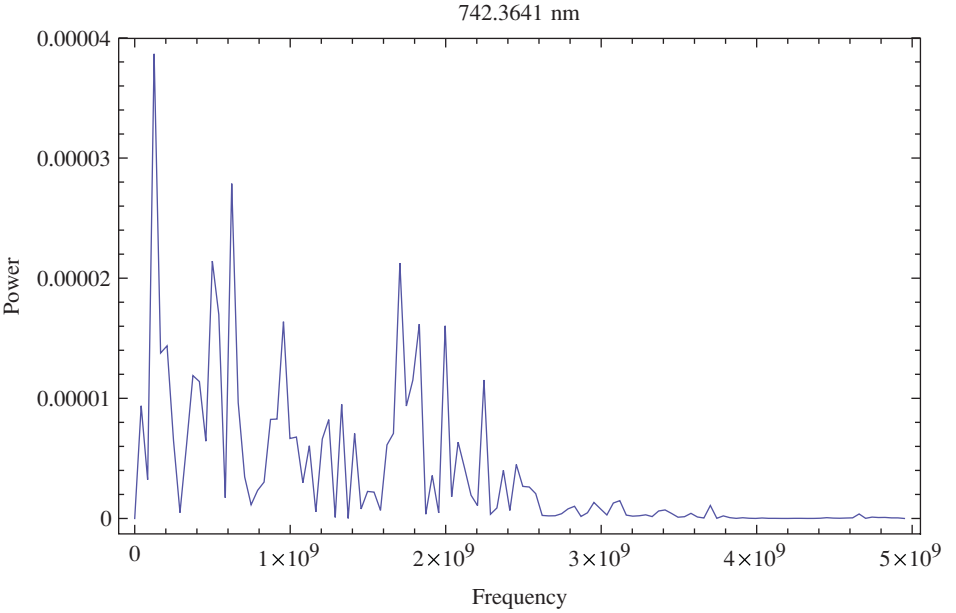

(b)

Figure 4. (Colour online) These plots show the effect that the cw laser has on the characteristic frequency as it changes from (a) 96 W cm^{-2} to (b) 286 W cm^{-2} for the neutral nitrogen line.

https://doi.org/10.1017/S0022377810000656 Published online by Cambridge University Press

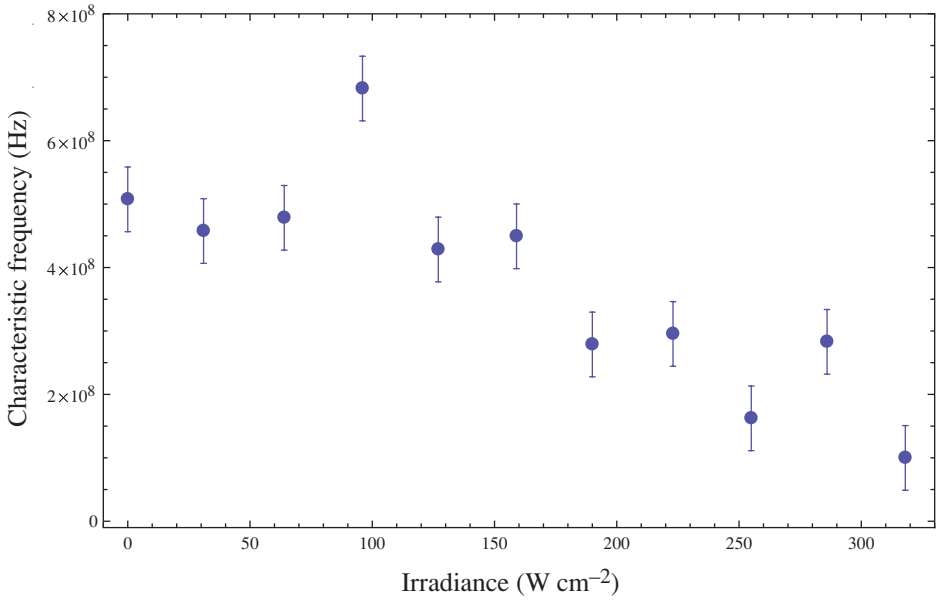

Figure 5. (Colour online) This plot shows a decrease in the characteristic frequency due to the changes in the cw fiber laser irradiance for neutral nitrogen lines. The standard deviation is $\pm 5.1 \times 10^7$Hz and has a 13.6% error.

behavior shown in Fig. 9, which is a clear indication of a second-order transformation in the turbulence of the laser-induced plasma. From the approximate lambda-like profiles we can identify critical turbulent energies in the data. In this context, these critical turbulent energies identify the turbulent energy when the plasmas are in turbulent transitional equilibrium [8] where the plasma goes from a non-turbulent state to a turbulent state. Fig. 10 shows the behavior of the critical turbulent energies for both the neutral and ion nitrogen line as the cw laser irradiance changes. There one sees that the critical turbulent energy from the spectral index for the neutral line remained fairly constant and the changes to the critical turbulent energy was modest for the ion line.

5. Conclusion

We have shown the effects that a cw laser has on the turbulent environment of laser-induced plasmas are well beyond the predictive powers of current theoretical physics. We have shown that as the cw laser irradiance changes, the complexity of the plasma also increase for the neutral line. The cw laser reduces the characteristic fluctuation frequencies in the neutral lines. We observed a clear shift in the position of the strongest peak frequency as the cw laser irradiance changed for the neutral line. We have shown that the turbulent energy of the ionic line increases and the turbulent energy decreases for the neutral nitrogen line. We have shown that from the approximate lambda like profiles of the transport parameter verses the turbulent energy we can identify when the plasma undergoes a transition to turbulence.

https://doi.org/10.1017/S0022377810000656 Published online by Cambridge University Press

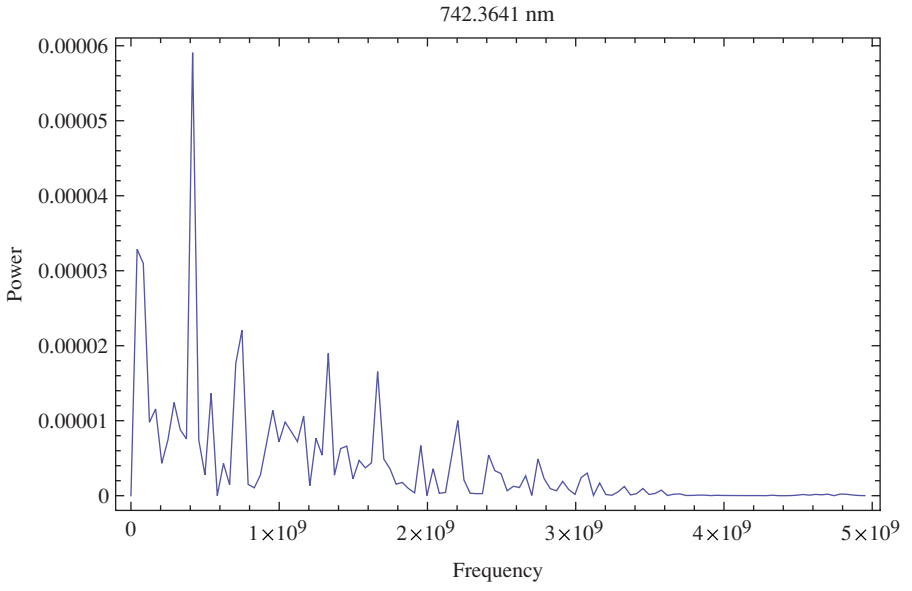

(a)

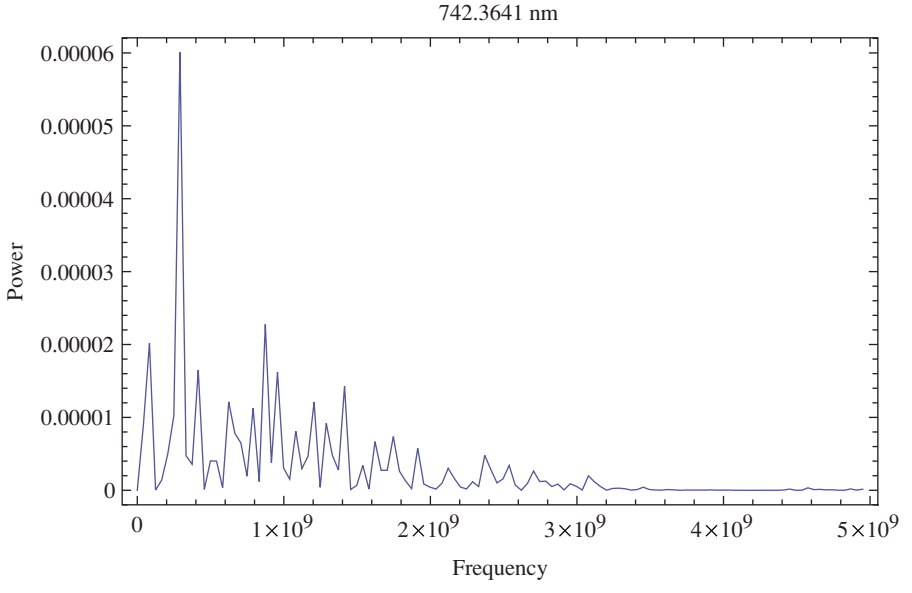

(b)

Figure 6. (Colour online) These plots show that the area under the curve decreases at $t = 200$ ns as the cw laser irradiance changes from (a) 96 W cm^{-2} and (b) 286 W cm^{-2} for the nitrogen neutral line.

https://doi.org/10.1017/S0022377810000656 Published online by Cambridge University Press

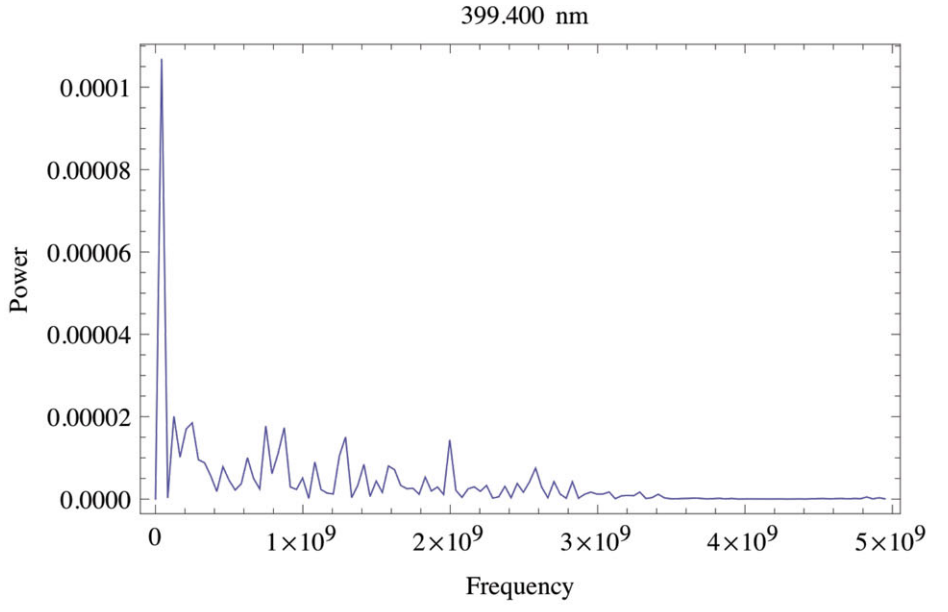

(a)

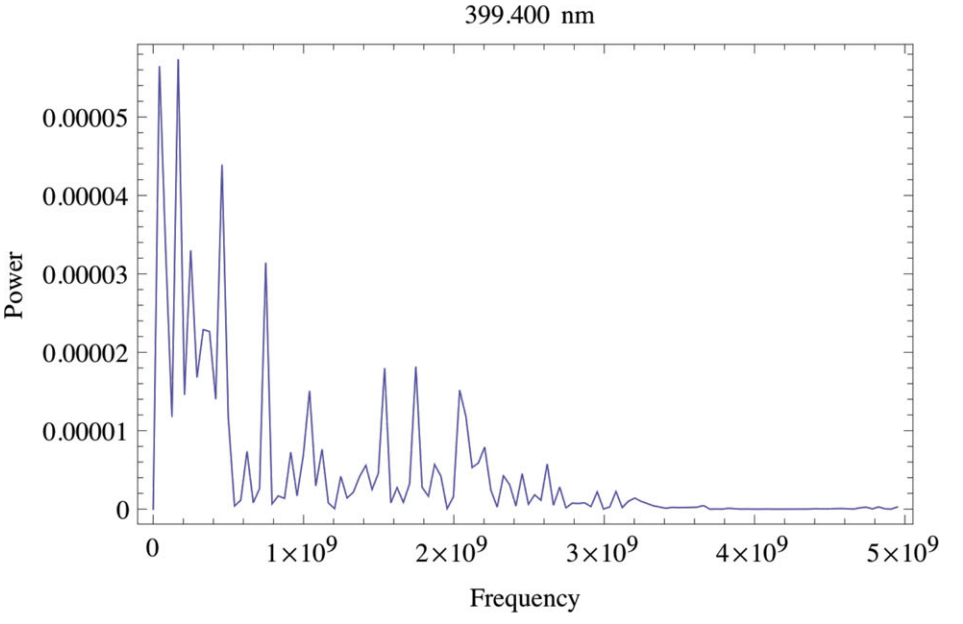

(b)

Figure 7. (Colour online) These plots show that the area under the curve increases at $t = 200$ ns as the cw laser irradiance changes from (a) 96 W cm^{-2} and (b) 286 W cm^{-2} for the nitrogen ion line.

https://doi.org/10.1017/S0022377810000656 Published online by Cambridge University Press

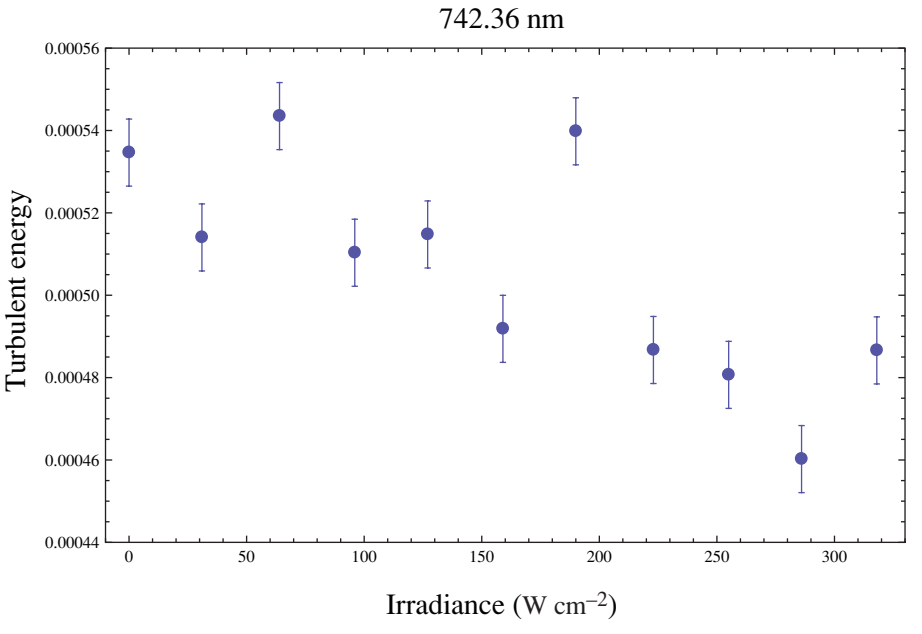

(a)

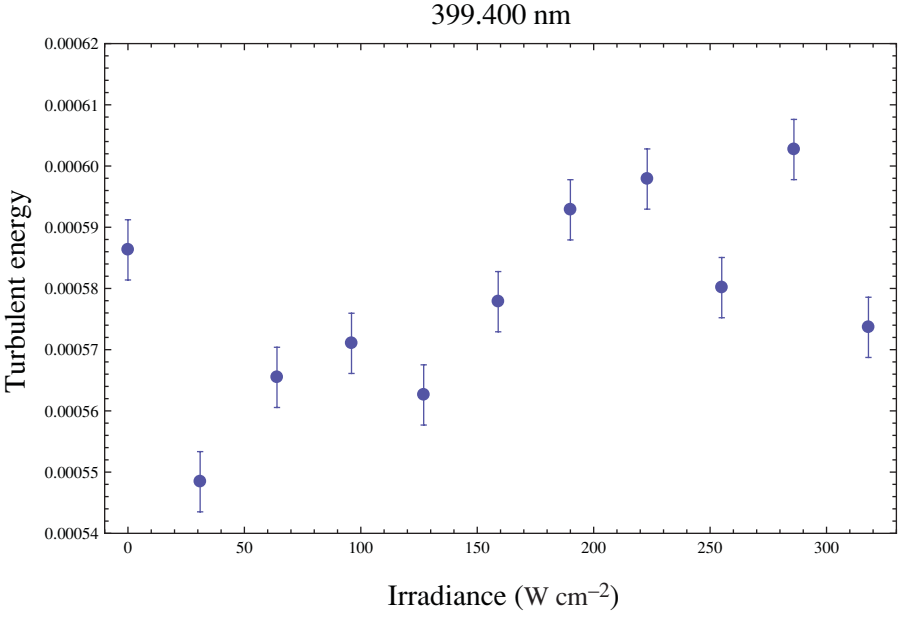

(b)

Figure 8. (Colour online) These plots show that the turbulent energy decreases for the (a) neutral line and increases for the (b) ion line. The standard deviation for the neutral line is $\pm 8.14 \times 10^{-6}$ and has a 1.61% error. The standard deviation for the ion line is $\pm 4.92 \times 10^{-6}$ and has a 0.85% error.

https://doi.org/10.1017/S0022377810000656 Published online by Cambridge University Press

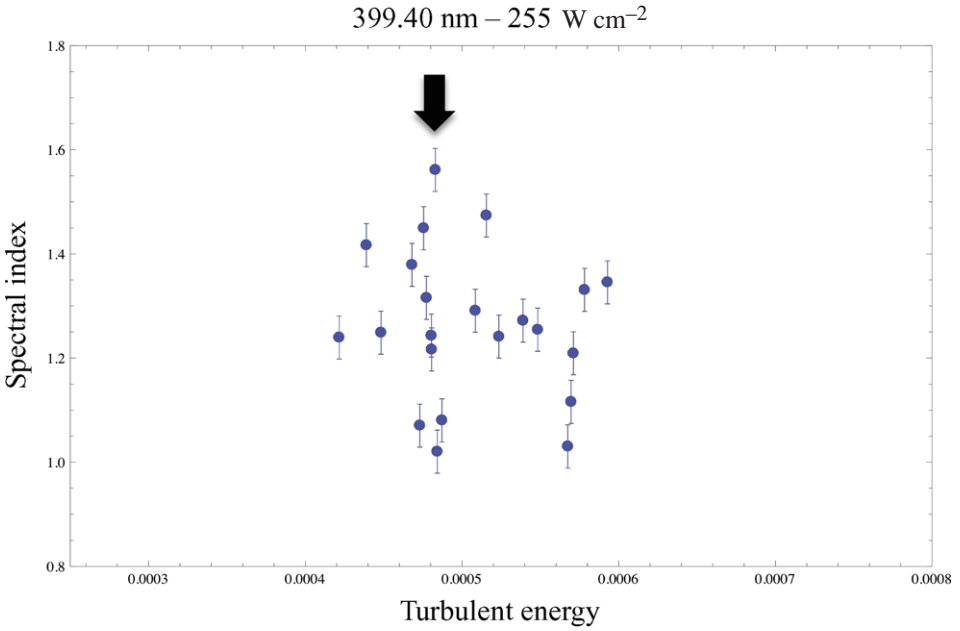

(a)

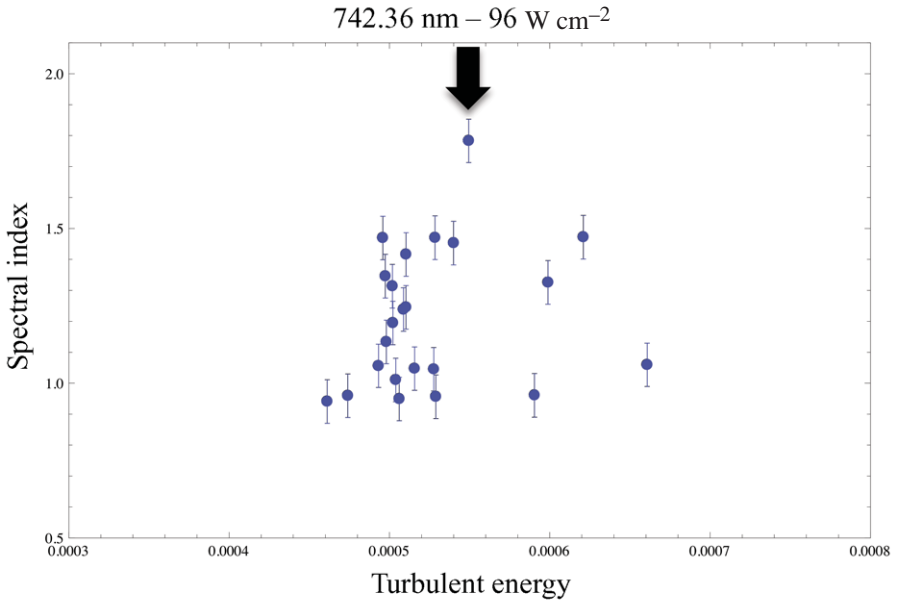

(b)

Figure 9. (Colour online) These plots show an approximate lambda-like profile for the spectral index versus turbulent energy for both the (a) neutral and (b) ion nitrogen lines for a fixed irradiance. The critical turbulent energy is identified with the arrows.

https://doi.org/10.1017/S0022377810000656 Published online by Cambridge University Press

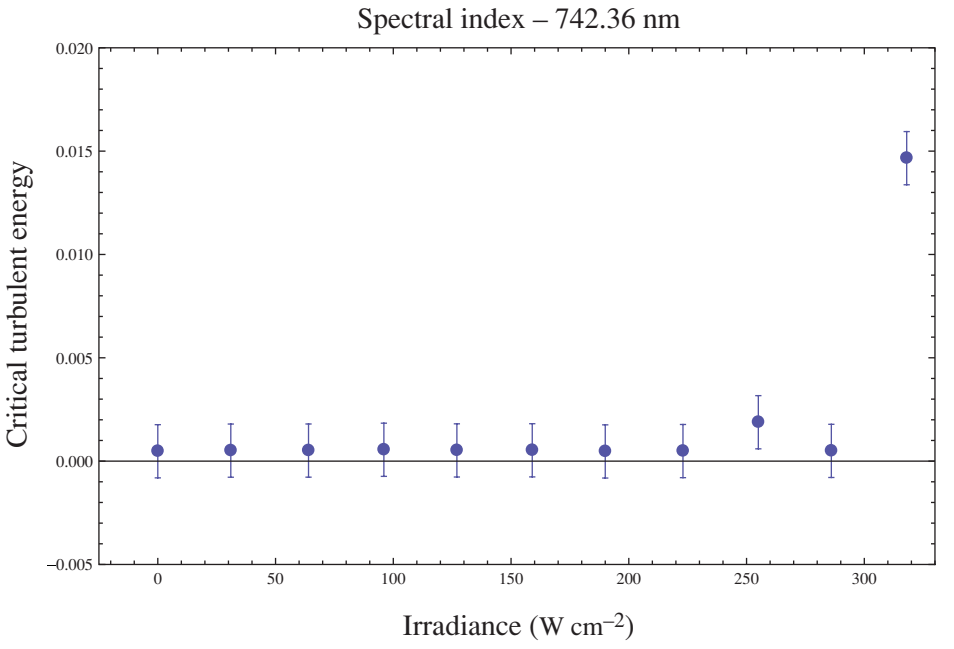

(a)

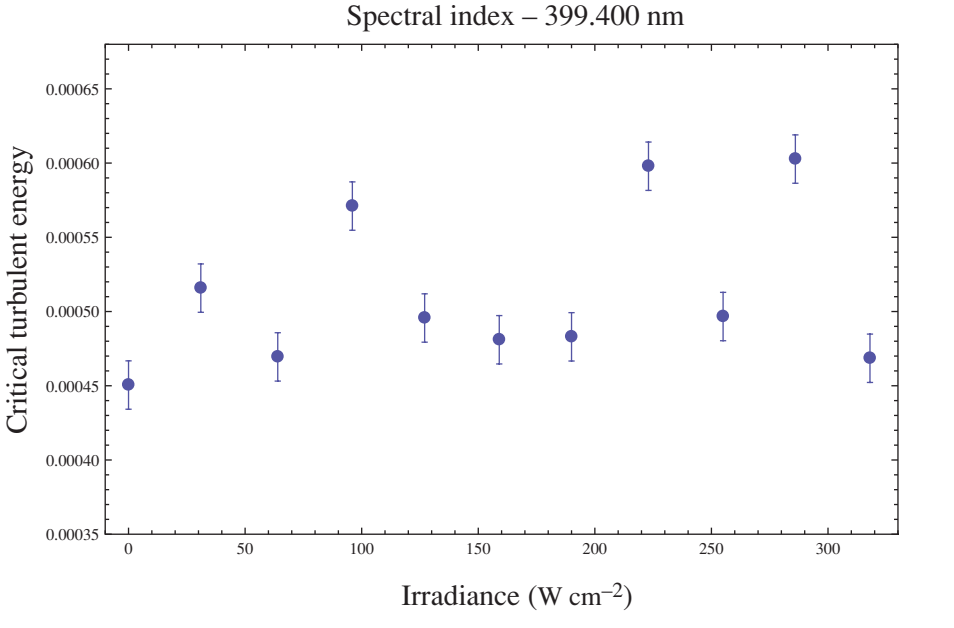

(b)

Figure 10. (Colour online) These plots show the behavior of the critical turbulent energies as the cw laser irradiance changes for the (a) neutral nitrogen line and (b) the ion nitrogen line. The standard deviation for the neutral line is $\pm 1.92 \times 10^{-3}$ and has a 67.15% error. The standard deviation for ion line is $\pm 1.62 \times 10^{-5}$ and has a 3.18% error.

https://doi.org/10.1017/S0022377810000656 Published online by Cambridge University Press

Acknowledgements

This research was supported in part by funding from the Department of Defense (SMDC) and the National Science Foundation to Florida A & M University.

References

[1] Johnson, III, J. A., Lin, I. and Santiago, J. P. 1990 Turbulent collisional ionizing shock waves in argon. *J. Phys. D: Appl. Phys.* **23**, 662–672.

[2] Belay, K., Valentine, J. M., Williams, R. L. and Johnson III, J. A. 1997 Interaction of turbulent plasma flow with a hypersonic shock wave. *J. Appl. Phys.* **81** (3), 1073–1076.

[3] Podder, N. K., Mezonlin, E.-D. and Johnson III, J. A. 2002 Turbulent microwave plasma thermodynamics for fundamental fluctuation modes. *Phys. of Plasma* **9**, 8, 3364–3368.

[4] Roberson, S. D., Akpovo, C., Mezonlin, E.-D. and Johnson III, J. A. 2008 Evidence of turbulence in laser-induced plasmas. *J. Appl. Phys.* **103**, 053307, 1–16.

[5] Choudhui, A. R. 1998 *The Physics of Fluids and Plasma: An Introduction for Astrophysicists*. Cambridge University Press, pp. 174.

[6] Landau, L. D. and Lifshitz, E. M. 1987 *Fluid Mechanics*. Reed Educational and Professional Ltd., pp. 130.

[7] Williams, K. M., Podder, N. K. and Johnson III, J. A. 2004 Universality in turbulence using turbulent energy concepts in moving and stationary plasmas. *Phys. Lett.* A **331**, 1, 70–76.

[8] Annett, J. P. 2004 *Superconductivity, Superfluids, and Condensates*. Oxford University Press, Vol. 67, pp. 71–74.

[9] Shuster, H. G. 1995 *Deterministic Chaos*. D-69451 Weinheim: VCH Verlagsgesellschaft mbH, pp. 54–55.

[10] Grassberger, P. and Procaccia, I. 1983 Characterization of Strange Attractors. *Phys. Rev. Lett.* **50**, 5, 346–349.

[11] Frisch, U. 1998 *Turbulence*. Cambridge, UK: Cambridge University Press, pp. 92–99.

[12] Numasato, R., Tsubota, M. and L'vov, V. S. 2010 Direct energy cascade in two-dimensional compressible quantum turbulence. *Phys. Rev.* A **81**, 063630, 1–12.

[13] Boffetta, G. and Musacchio, S. 2010 Evidence for the double cascade scenario in two-dimensional turbulence. *Phys. Rev.* E **82**, 016307, 1–5.

[14] Numasato, R., Tsubota, M. and L'vov, V. S. 2010 Direct energy cascade in two-dimensional compressible quantum turbulence. *Phys. Rev.* A **81**, 063630, 1–12.

[15] Boffetta, G. and Musacchio, S. 2010 Evidence for the double cascade scenario in two-dimensional turbulence. *Phys. Rev.* E **82**, 016307, 1–5.

[16] Tenekes, H. and Lumley, J. L. 1972 *A First Course in Turbulence*. Cambridge, Massachusetts: The MIT Press, pp. 300.

[17] Wiggins, D. L., Raynor, C. T. and Johnson III, J. A. 2010 Evidence of inverse bremsstrahlung in laser enhanced laser-induced plasma. *Phys. of Plasma*, **17**, 1, 1–6.